UNCLASSIFIED

SECURITY CLASSIFICATION OF THIS PAGE (When Data Entered)

# REPORT DOCUMENTATION PAGE

READ INSTRUCTIONS BEFORE COMPLETING FORM

| | |
|---|---|
| 1. REPORT NUMBER: AFOSR-TR-81-0393 | 2. GOVT ACCESSION NO. |
| 3. RECIPIENT'S CATALOG NUMBER | |
| 4. TITLE (and Subtitle): Predicted and Measured Effects of Pressure and Crossflow Velocity on Composite Propellant Burning Rate | 5. TYPE OF REPORT & PERIOD COVERED: Interim rept. |
| 6. PERFORMING ORG. REPORT NUMBER | |
| 7. AUTHOR(s): Merrill K. King | 8. CONTRACT OR GRANT NUMBER(s): F49620-78-C-0016 |
| 9. PERFORMING ORGANIZATION NAME AND ADDRESS: Atlantic Research Corporation, 5390 Cherokee Avenue, Alexandria, VA 22314 | 10. PROGRAM ELEMENT, PROJECT, TASK AREA & WORK UNIT NUMBERS: 2308A1, 61102F, 26 |
| 11. CONTROLLING OFFICE NAME AND ADDRESS: Air Force Office of Scientific Research/NA, Building 410, Bolling AFB, DC 20332 | 12. REPORT DATE: Dec 80 |
| | 13. NUMBER OF PAGES: 24 |
| 14. MONITORING AGENCY NAME & ADDRESS(if different from Controlling Office) | 15. SECURITY CLASS. (of this report): Unclassified |
| | 15a. DECLASSIFICATION/DOWNGRADING SCHEDULE |

16. DISTRIBUTION STATEMENT (of this Report)

Approved for public release; distribution unlimited.

17. DISTRIBUTION STATEMENT (of the abstract entered in Block 20, if different from Report)

DTIC ELECTE APR 23 1981 D A

18. SUPPLEMENTARY NOTES

19. KEY WORDS (Continue on reverse side if necessary and identify by block number)

Erosive Burning
Composite Propellants
Propellant Combustion Modeling
Solid Propellant Combustion

20. ABSTRACT (Continue on reverse side if necessary and identify by block number)

A theoretical model for prediction of burning rates of composite (ammonium perchlorate oxidizer) solid propellants as a function of pressure and crossflow velocity has been developed. Included in this model is the capability for treatment of multimodal oxidizer particle sizes and metalized formulations. In addition, an experimental device for measuring the effects of crossflow velocity on propellant burning rate has been developed and used

(over)

DD FORM 1 JAN 73 1473 EDITION OF 1 NOV 65 IS OBSOLETE

UNCLASSIFIED 045550

SECURITY CLASSIFICATION OF THIS PAGE (When Data Entered)

AD A098090

DTIC FILE COPY

to characterize a series of AP/HTPB propellants with systematically varied formulation parameters. Model predictions of zero-crossflow burning rate versus pressure characteristics have been found to be in excellent agreement with data, while the agreement between erosive burning predictions and data is in general good. The experimental data indicate that the dominant factor influencing the sensitivity of composite propellant burning rate to crossflow is the base (no-crossflow) burning rate versus pressure characteristics of the propellant (lower base burning rate leading to increased crossflow sensitivity) with other factors having at most a second order effect outside their influence on base burning rate. For example, three formulations with widely different compositional and ingredient particle size parameters but with nearly identical base burning characteristics exhibited very similar erosive burning characteristics. Finally, the model has been used to examine the effects of motor scaling on erosive burning: erosive burning is predicted to diminish with increasing motor size, in agreement with experience.

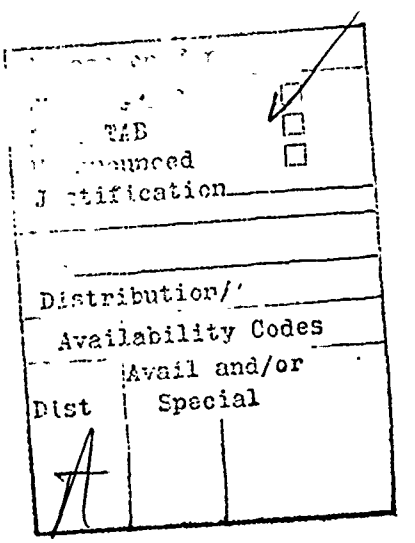

# PREDICTED AND MEASURED EFFECTS OF PRESSURE AND CROSSFLOW VELOCITY ON COMPOSITE PROPELLANT BURNING RATE*

Merrill K. King
Atlantic Research Corporation
Alexandria, Virginia 22314

## ABSTRACT

A theoretical model for prediction of burning rates of composite (ammonium perchlorate oxidizer) solid propellants as a function of pressure and crossflow velocity has been developed. Included in this model is the capability for treatment of multimodal oxidizer particle sizes and metalized formulations. In addition, an experimental device for measuring the effects of crossflow velocity on propellant burning rate has been developed and used to characterize a series of AP/HTPB propellants with systematically varied formulation parameters. Model predictions of zero-crossflow burning rate versus pressure characteristics have been found to be in excellent agreement with data, while the agreement between erosive burning predictions and data is in general good. The experimental data indicate that the dominant factor influencing the sensitivity of composite propellant burning rate to crossflow is the base (no-crossflow) burning rate versus pressure characteristics of the propellant (lower base burning rate leading to increased crossflow sensitivity) with other factors having at most a second order effect outside their influence on base burning rate. For example, three formulations with widely different compositional and ingredient particle size parameters but with nearly identical base burning characteristics exhibited very similar erosive burning characteristics. Finally, the model has been used to examine the effects of motor scaling on erosive burning: erosive burning is predicted to diminish with increasing motor size, in agreement with experience.

## INTRODUCTION AND BACKGROUND

Erosive burning, the alteration of propellant burning rate by high velocity product flow across the burning surface, has become an increasingly important phenomenon with the advent of very low port-to-throat area ratio cylindrically perforated motors and nozzleless motors. The motor designer must be able to predict this burning rate modification and in particular understand the effects of motor scaling and length/diameter ratio on erosive burning in order to properly carry out his function. In addition, the propellant chemist needs to understand the effects of various formulation parameters on the sensitivity of a propellant to crossflow in order to tailor propellants to desired ballistic characteristics.

---

*Research sponsored by the Air Force Office of Scientific Research (AFSC), United States Air Force, under Contract F49620-78-C-0016. The United States Government is authorized to reproduce and distribute reprints for Governmental purposes notwithstanding any copyright notation hereon.

Over the past several years, this investigator has been conducting an experimental and analytical study of the erosive burning of composite propellants with the aims of determining how various formulation parameters influence the sensitivity of propellant burning rate to crossflow, developing an *a priori* burning rate model (second generation model) which will permit accurate prediction of composite propellant burning rate as a function of pressure and crossflow velocity given only the formulation composition and solid ingredient particle sizes, and developing scaling laws to permit extrapolation of erosive burning data obtained in test devices and small motors to larger motor situations. Details of the model development, with the exception of the treatment of effects of aluminum additive on burning rate, are presented in References 1 and 2. During the past year, the model has been slightly modified to more accurately treat the augmentation of transport properties by crossflow-induced turbulence, and it has been extended to treat aluminized formulations as well as non-metalized ones.

Since there is a dearth of systematic experimental erosive burning data in the literature, a test device has been developed and used to characterize the erosive burning behavior of a series of AP/HTPB composite propellants with systematically varied formulation properties. Zero-crossflow predictions and data have been generated for thirteen non-catalyzed AP/HTPB formulations (four containing aluminum) while crossflow data and predictions have been obtained for ten of these formulations to date. A brief description of the model (with emphasis on its extension to treat metalized propellants), comparison of theoretical predictions with data, and definition of major parameters affecting composite propellant crossflow sensitivity are presented in the following sections.

## MODEL DESCRIPTION

The major elements involved in development of a complete *a priori* model for prediction of composite propellant burning rate as a function of pressure and crossflow velocity include development of a no-crossflow composite propellant model (embodying many of the concepts of the Beckstead-Derr-Price[3] model) for prediction of burning rate as a function of pressure in the absence of crossflow, followed by incorporation of modifications based on two postulated mechanisms for augmentation of heat feedback from flames in the gas phase above the propellant surface by crossflow. (See Figure 1). As discussed in Reference 2, several variants of a basic no-crossflow model were developed for unimodal-oxidizer non-metalized propellants, with one variant finally being selected for extension to treatment of formulations containing multimodal oxidizer and metal fuel.

The basic model centers around an energy balance at the propellant surface. In this balance, the product of the propellant burning mass flow and the heat required to raise the ingredients from ambient temperature to the surface temperature (related to the burning rate by an Arrhenius function) plus the heat required to vaporize that fraction of the ingredients which do not exothermically react just below the surface is equated to the sum of the heat release rate from subsurface reactions and the rate of heat feedback from the two gas flame zones depicted in Figure 1. (For metalized formulations, as discussed later, an additional heat release zone associated with burning of the metal in the gas above the propellant surface, not depicted in Figure 1, is also considered.) Thus, the burning rate of non-metalized formulations is

controlled by three principal heat release zones: (1) heat release in a thin subsurface zone just adjacent to the propellant surface; (2) heat release in the gas phase above the propellant from ammonium perchlorate decomposition products burning as a nonpropellant; and (3) heat release from a diffusion flame between the AP decomposition (and monopropellant flame) products and fuel vapor released by binder pyrolysis.

The subsurface heat release is calculated by an iterative process, coupled with the remainder of the model, in which an estimate of the subsurface temperature profile is made and substituted into an Arrhenius rate expression representing subsurface heat release data measured by Waesche and Wenograd[4], which is then integrated from the surface to a depth where the temperature drops below the melting point of AP to obtain the total subsurface heat release per unit mass of propellant. This is then multiplied by the burning mass flux to yield a heat release rate. This procedure differs markedly from that of the BDP model in which the amount of subsurface heat release per unit mass of propellant is assumed to be a constant, independent of such parameters as burning rate, and is included with the binder heat of vaporization. Since the subsurface temperature profile steepens rapidly with increasing burning rate, while surface temperature increases with burning rate, the procedure used herein results in the subsurface heat release per unit mass of propellant varying with the burning rate.

For the gas phase, a two-flame approach was chosen for this model, the two flames being an AP monopropellant flame and a columnar diffusion (Burke-Schumann[5]) flame. As indicated in Figure 1, three distance parameters ($FH90\sin\theta$, $L_{AP}$, and $L_{RX}$) are important in calculating heat feedback from these gas flames to the propellant surface. FH90 refers to the distance associated with completion of mixing of 90 percent of the fuel and oxidizer gas products, while $L_{RX}$ and $L_{AP}$ are reaction distances (products of reaction times and gas velocity away from the surface) associated with the binder gas-oxidizer gas flame and the monopropellant AP gas flame, respectively. As discussed below, flame bending associated with crossflow is postulated to reduce the distance from the surface to the end of the mixing region, measured perpendicular to the surface, by the factor $\sin\theta$, where $\theta$ is the angle between the surface and the resultant vector of the transpiration and crossflow velocities.

Heat release from the AP monopropellant flame is assumed to occur at one plane, resulting in a discontinuity in the temperature derivative at its point of release, while the columnar diffusion flame is assumed to release its heat in a distributed fashion (the distribution being defined by a Burke-Schumann[5] analysis) between distances $L_{RX}$ and $L_{RX} + FH90\sin\theta$ from the surface.

Details of the equation development for the unimodal oxidizer, non-metalized propellant model and the solution procedure are presented in References 1 and 2. Included in the model are three "free" constants to be chosen by optimization against data. These three constants are pre-exponentials associated with the subsurface heat release rate expression and the two rate expressions used to calculate the gas-phase reaction times. These constants were chosen on the basis of no-crossflow burning rate versus pressure data for four unimodal oxidizer AP/HTPB (hydroxyterminated polybutadiene) formulations and then used unchanged for no-crossflow and crossflow calculation for multimodal oxidizer and metalized formulations.

Extension of the basic model to treat multimodal oxidizer propellants was carried out in a very straightforward manner using a minor variation on Glick's "petit ensemble" approach[6]. In Glick's approach, a propellant containing oxidizer particles of different sizes is broken into a series of subpropellants, each of which contains oxidizer of only one size. The subpropellents are assumed to burn non-interactively, with the unimodal oxidizer model being used to calculate a mass flux for each, and straightforward averaging weighted according to fractional surface areas associated with each subpropellant then being used to obtain an overall propellant average linear regression rate. The only manner in which oxidizer of one size is allowed to affect the burning rate of a subpropellant containing oxidizer of another size is through possible influence on the assignment of fuel to that subpropellant. That is, rather than fuel having to be assigned to each oxidizer size category in direct proportion to the amount of oxidizer in that category, the capability of allowing uneven assignment of fuel to various oxidizer size subpropellants is included by means of a power law:

$$V_{f,d_i} = C_2 \, (D_o)^{XEXPOF} \tag{1}$$

where $V_{f,d_i}$ is the volume of fuel assigned to a particle of diameter $(D_o)_i$, XEXPOF is an arbitrary input power law constant, and $C_2$ is a constant determined by application of overall continuity. It may easily be shown that XEXPOF = 3 will result in each subpropellant having the same oxidizer/fuel ratio as the overall propellant. XEXPOF<3, on the other hand, will result in subpropellants with small oxidizer being more fuel-rich than the overall propellant and subpropellants with large oxidizer being more fuel-lean, with the reverse occurring for XEXPOF>3. (Based on preliminary calculations, XEXPOF has been set equal to 3 in the calculations presented herein.)

As mentioned, one modification to the Glick approach has been introduced. His averaging procedure involves an implicit assumption that the average fractional surface area of the total propellant which is subpropellant i is equal to the volume fraction of the propellant which is subpropellant i. However, careful examination of the situation indicates that if there are subpropellants burning at different rates, the slower burning ones will at any given time occupy a higher fraction of the surface than indicated by their volume fraction: thus, it seems that an averaging approach based on residence time distributions is more appropriate. Development of this concept leads to the average burning rate for XEXPOF=3 cases being given by:

$$\bar{r} = 1/\Sigma x_i/r_i \tag{2}$$

rather than by Glick's formula:

$$\bar{r} = \Sigma x_i r_i \tag{3}$$

$r_i$ = burning rate of subpropellant i

$x_i$ = mass fraction of propellant in subpropellant i

$\bar{r}$ = average burning rate

The model described in detail in Reference 2 has recently been extended to treat the effects of aluminum additive on propellant burning rate. The metal is allowed to affect burning rate both through heat sink effects (altered

heatup terms in the overall energy balance and a depressed gas diffusion flame temperature relative to that which would be achieved by the oxidizer and fuel in the absence of the metal heat sink) and via conductive and radiative feedback of heat released by the metal particles burning with the gas flame products above the propellant surface. Among the phemonema treated in this model are aluminum agglomeration at the surface, particle velocity lag relative to the gases leaving the propellant surface, particle ignition delay, particle combustion, conductive feedback from incremental heat release zones at various distances from the propellant surface, and radiative feedback. In the case of multimodal oxidizer propellants, the assignment of various fractions of the aluminum to the various subpropellants is treated in the same manner as the assignment of fuel (binder) to these subpropellants. (As with the assignment of binder to subpropellants containing different size oxidizer particles, in the calculations presented herein, the assignment of metal was carried out such that all subpropellants were of the same composition as the overall formulation.)

Aluminum particles are assumed to leave the propellant surface in two forms, agglomerated and unagglomerated (virgin), with the agglomerate fraction and size being calculated using empirical formulae developed by Beckstead[7].

$$D_{AG} = MAX\left(D_{UN}, \left[(1-\epsilon)\frac{\zeta_{Al}}{\zeta_{OX,C}}\right]^{1/3} D_{OX,C}\right) \quad (4)$$

$$\epsilon = 1-0.0005\, D_{OX,C}\, D_{UN}^{0.25}\left[\frac{1+30(F/C)}{1+80(F/C)^2}\right] \quad (5)$$

$\epsilon$ = Fraction aluminum not agglomerated

$D_{AG}$ = Agglomerate diameter (microns)

$D_{UN}$ = Virgin metal diameter (microns)

$D_{OX,C}$ = Coarse fraction oxidizer diameter (microns)

$\zeta_{Al}$ = Volume fraction Aluminum in Propellant

$\zeta_{OX,C}$ = Volume Fraction Coarse Oxidizer in Propellant

F/C = Weight of Finest Oxidizer Cut/Weight of Coarsest Oxidizer Cut

Based on preliminary calculations, agglomerates were assumed to contribute negligible conductive feedback to the proepllant surface due to long ignition and combustion times. Ignition delay times for virgin particles subsequent to leaving the surface are calculated from a simple heatup formula:

$$t_{ign} = \frac{\rho_{Al}\, D_{UN}^2}{12\,\lambda_{gas}}\left[C_{p,Al}\ln\left(\frac{T_{Final}-T_s}{T_{Final}-T_{ign}}\right)+\frac{L_{melt}}{T_{Final}-T_{melt}}\right] \quad (6)$$

$t_{ign}$ = Ignition delay time

$\rho_{Al}$ = Aluminum particle density

$\lambda_{gas}$ = gas thermal conductivity

$C_{p,Al}$ = Aluminum specific heat

$T_{Final}$ = Equilibrium flame temperature subsequent to Al combustion

$T_s$ = Propellant Surface Temperature

$T_{ign}$ = Aluminum particle ignition temperature (2100°K)

$T_{melt}$ = Aluminum melting temperature

$L_{melt}$ = Aluminum heat of fusion

After ignition, the particle diameter-time history (and thus burning rate) is calculated using a rearranged form of the Belyaev [8] burning time formula:

$$D_{t+\Delta t} = \left[D_t^{1.5} - (a_k^{0.9}/670)\,\Delta t\right]^{0.667} \qquad (7)$$

$D_t$ = particle diameter (cm) at time t

$D_{t+\Delta t}$ = particle diameter at time $t+\Delta t$

$\Delta t$ = time increment (seconds)

$a_k$ = $100\,(n_{CO_2} + n_{H_2O} + n_{O_2})/\Sigma n_i$

Thus, from Equations 6 and 7, the fractional consumption of aluminum as a function of time subsequent to its leaving the surface is calculated. (Note that implicit in Equation 6 is an assumption that the aluminum particle temperature is equal to the propellant surface temperature when it leaves the surface.)

For calculation of the distance of the particle from the surface versus time (required for calculation of the metal heat release distribution) the gas velocity component normal to the surface is first calculated as a function of distance from the surface using the propellant burning flux calculated in the previous loop of the overall trial and error solution procedure along with assumption of a linear temperature profile from the propellant surface to the end of the columnar diffusion flame zone with subsequent constant temperature. Next, a force balance on the particle (with a buoyancy term neglected on the basis of preliminary estimates for particle sizes of interest):

$$\frac{\Delta V_p}{\Delta t} = \frac{0.75\,\rho_g\,C_D\,(V_g - V_p)^2}{\rho_{Al}\,D} \qquad (8)$$

$\Delta V_p$ = change in particle velocity in time increment $\Delta t$

$\rho_g$ = gas density

$C_D$ = drag coefficient

$V_g$ = gas velocity component normal to surface

$V_P$ = particle velocity component normal to surface

D = particle diameter

is integrated outward from the surface, utilizing a fitted drag coefficient versus Reynolds' Number expression, with this coefficient assumed (based on the work of Marshall [9]) to increase by a factor of 2.5 for ignited particles. (Actually, Equations 7 and 8 have to be integrated simultaneously subsequent to particle ignition since they are coupled through the changing particle diameter.) With coupling of Equations 5-8, the fraction of the total aluminum in the propellant burned is calculated as a function of distance from the propellant surface. This is then multiplied by the heat of combustion of aluminum in the oxidizer/fuel products, calculated as:

$$Q_{AL} = c_{pm} (T_{Final} - T^*)/X_{Al} \qquad (9)$$

$Q_{Al}$ = aluminum heat of combustion per unit mass

$C_{pm}$ = mixture specific heat

$T^*$ = equilibrium flame temperature with non-reacting aluminum

$X_{Al}$ = weight fraction aluminum in the propellant

to yield a distribution of heat release from aluminum combustion versus distance from the propellant surface. Conductive feedback flux from the aluminum combustion to the propellant surface is then calculated from:

$$q_{fdbk,Al,c} = \dot{m} \sum_j \left[ Q_j \prod_{i=1}^{j} \exp(-\dot{m} c_p \Delta x_i / \lambda_i) \right] \qquad (10)$$

$\dot{m}$ = propellant burning mass flux ($gm/cm^2 sec$)

$q_{fdbk,Al,c}$ = aluminum feedback flux $cal/cm^2 sec$)

$Q_j$ = aluminum heat release per unit mass of propellant at jth node from the surface (cal/gm)

$C_p$ = product heat capacity

$\Delta x_i$ = size of ith increment

$\lambda_i$ = total thermal conductivity (laminar plus turbulent) associated with ith increment

Preliminary calculations indicated that radiative feedback should in general be small, but a very simplified analysis for estimating this feedback was included. In this analysis, an effective distance from the surface is input as a free parameter and an effective cloud emmisivity based on the fractional area subtended by particles in that region is then calculated: for motors, the distance is chosen to be the port radius while for strands it is arbitrarily set equal to 1 to 2 centimeters (with the assumption that cooling due to entrained nitrogen from the surroundings makes particles further away ineffective). For the metalized formulations tested and discussed in this paper, radiative transfer is predicted to have an insignificant effect on predicted burning rate.

It was originally postulated by this author that the augmentation of composite propellant burning rate due to crossflow resulted solely from shortening of the distance, measured normal to the propellant surface, associated with mixing of the fuel and oxidizer gases through distortion of the mixing cone, as depicted in Figure 2. A detailed discussion of this mechanism is given in Reference 10. From tall-flame theory, for no crossflow, the mixing distance is related to the burning mass flux and oxidizer particle diameter by:

$$FH90 = k\,\dot{m}_p d_p^2 \tag{11}$$

With crossflow (refer to Figure 2) the mass flux in the direction of the resultant flow is:

$$\dot{m} = \dot{m}_p/\sin\theta \tag{12}$$

where $\theta$ is the resultant flow angle. However, the characteristic mixing time is decreased since the average mixing concentration gradient is increased by the circular mixing cross-section (in the absence of crossflow) being converted to an elliptical cross-section with major axis $d_p$ and minor axis $d_p\sin\theta$. An exact mixing calculation for this geometry is of course quite difficult, but replacement of the circle diameter $d_p$ by the geometric mean ellipse diameter, $\sqrt{d_p^2\sin\theta}$ in Equation 11 does not seem unreasonable. With substitution of (12) into (11), one finds:

$$FH90 = \frac{k\dot{m}_p}{\sin\theta}\ (d_p^2\ \sin\theta) = k\dot{m}_p\ d_p^2 \tag{13}$$

as in the case of no crossflow. However, this FH90 is now measured along the resultant flow vector: accordingly, the distance from the surface to the end of the mixing zone is reduced to $FH90\sin\theta$.

Use of an erosive burning package based solely on this mechanism in the different Generation 2 model variants led in all cases to major under-prediction of the effect of crossflow on burning rate, indicating that the flame-bending mechanism was by itself insufficient. Accordingly, a second possible mechanism, augmentation of turbulence transport properties in the region between the propellant surface and the gas-phase flames was invoked and combined with the flame-bending mechanism. In this approach, it was assumed that both the effective thermal conductivity (governing feedback from the various gas flames) and the effective mass diffusivity (an important parameter in determining the thickness of the diffusion flame) were increased in crossflow situations by crossflow-induced turbulence. A flow profile analysis

permitting calculation of eddy viscosity (and, by analogy, total effective thermal conductivity and diffusivity) as a function of distance from the propellant surface for a given crossflow velocity, transpiration velocity (determined by the propellant burning rate), and temperature field (depending on the location of gas-phase heat release zones) was developed and coupled with the combustion model for erosive burning calculations. An improved calculation of diffusion flame-bending angle was also incorporated in this analysis.

Details of the flow profile analysis procedures are presented in Reference 2. (A summary of the equations used and the solution procedure employed are given in Table I and II.) The outputs from this analysis are used to calculate:

$$\lambda_{effective}/\lambda_{laminar} = D_{effective}/D_{laminar} = 1+\rho\epsilon/\mu = F(y) \qquad (14)$$

That is, the ratio of total transport properties to laminar transport properties are calculated as a function of distance from the surface. Average total transport property values between appropriate zones are then calculated and substituted for the laminar values in the diffusional mixing equations and the heat feedback equations in the original model, revised burn rates and flame distances are calculated, and the procedure is repeated until convergence is achieved. As might be expected, this looping procedure is considerably more complex in the case of multimodal propellants than for unimodal propellants since solution of the individual subpropellant cases becomes interactive in the case of crossflow. This interaction occurs because there is only one boundary layer for the overall propellant (that is, one cannot calculate a different boundary layer profile for each subpropellant) with the boundary layer details being controlled by the average transpiration velocity, flame height, surface temperature, etc. for the overall propellant rather than by the individual values of these parameters for each subpropellant.

It should be noted that the procedures used for calculating average transport properties between zones from the distribution of these properties have been modified from those procedures used in calculation of predicted burning rates presented in References 2 and 11. In the earlier work, linear averaging was employed, while the modified procedure allows for the fact that the effect of the gas-phase heat release on burning rate decreases exponentially with the distance of that release from the surface. In addition, in calculation of results presented previously, the bent flame was approximated as being straight with the effective angle being determined by integration of the velocity vector profile from the surface to the end of the diffusion flame zone while the effects of flame curvature are included in the current model.

Several options for closure of the boundary layer analysis through specification of an eddy viscosity equation were built into the model: all entailed use of a Prandtl mixing-length expression of the general form:

$$\epsilon = .168\ (y+y_\Delta)^2\ (DF)^2\ du/dy \qquad (15)$$

where DF is a damping factor which is a function of such parameters as blowing ratio, axial pressure gradient, and roughness height while $y_\Delta$ is an offset factor dependent on roughness height. Most satisfactory results were found

with DF set equal to unity (no damping) and $y_0$ set equal to zero (no roughness effect).

## EXPERIMENTAL

The experimental test apparatus (Figure 3) and procedures for measuring burning rates with crossflow are described in detail in Reference 12. A cylindrically perforated "driver" grain whose length is chosen to give the desired operating pressure produces a high velocity gas flow through a transition section into a rectangular channel which contains the test grain. The test grain extends through the transition section to butt against the driver grain to eliminate leading edge effects. The test grain is approximately 40 cm long, 1.90 cm wide, and 2.50 cm deep (web) and burns only on the 1.90 cm face. The flow channel is initially 1.90 x 1.90 cm, opening up to 1.90 cm x 4.40 cm as the test propellant burns. For high crossflow velocity tests, the apparatus is operated without a nozzle while for lower velocity tests, a two-dimensional nozzle is employed.

The burning rate is directly measured by photographing the ablating grain with a high-speed motion picture camera through a series of four quartz windows located along the length of the test section. Frame by frame analysis of the films permits determination of instantaneous burning rate as a function of time at each of the four window locations.

For nozzled cases, the measured location of the burning propellant surface at each window as a function of time, together with the known constant throat area, permits straightforward calculation of the crossflow velocity as a function of time. However, the very sensitive dependence of Mach number on area ratio for $M > 0.5$ makes calculation of crossflow velocity from area ratio measurement quite poor for nozzleless cases. Accordingly, for these tests, stagnation pressure is determined at the aft end of the test section and used in combination with the driver chamber pressure for calculation of the stagnation pressure in the test section as a function of time and position. Static presure wall taps at each window location are used for measurement of static pressure as a function of time for both nozzled and nozzleless cases. From the static and stagnation pressure values determined as a function of time and position down the test section, crossflow Mach Number and velocity are calculated as a function of time at each window location in the test section for the nozzleless cases.

The erosive burning characteristics of a series of 11 AP/HTPB formulations (4 with unimodal AP and no catalyst or metal, 5 with multimodal AP and no catalyst or metal, 1 with multimodal AP and aluminum but no catalyst, and 1 with unimodal AP plus catalyst) with systematically varied parameters have been measured in this device to date. In addition, standard strand-burning procedures have been used to determine zero-crossflow burning rate versus pressure characteristics for these 11 formulations plus 3 additional multimodal AP, aluminized (no catalyst) formulations. The propellant matrix tested, including the rationale for its selection, is presented in Table III.

## EXPERIMENTAL RESULTS AND COMPARISON WITH MODEL PREDICTIONS

Predicted and measured zero-crossflow burning rate versus pressure characteristics of 13 of the 14 formulations are presented in Figure 4-6.

(Predictions were not made for the catalyzed formulation since the catalyst should cause shifting of one or more of the three aforementioned kinetic constants and it was felt that the catalyzed formulation data base was insufficient for re-evaluation of these constants.) As may be seen, agreement between predicted and measured 200 psia burning rates is excellent, with all predictions, covering a wide range of non-metalized and metalized AP/HTPB formulations, falling within 10 percent of the measured values. Similarly, the 1000 psia burning rate predictions and data show excellnt agreement, with only one point falling outside the 20 percent error band and one falling between the 10 and 20 percent bands, the remainder agreeing within 10 percent. As indicated by Figure 6, the 1000 psia predicted versus measured value comparisons of burning rate pressure exponent are also quite good, all lying within the 20 percent error bands and most within the 10 percent bands. Accordingly, it appears that development of an accurate zero-crossflow model, necessary as a first step in developing an adequate erosive burning model, has been satisfied.

Erosive burning test results are presented in Figures 7-17, in the form of burning rate versus pressure at various crossflow velocities. In addition, theoretical predictions are presented for all but the catalyzed formulation (4869) in these figures. As may be seen, the agreement between data and predictions for the no-crossflow conditions is excellent, as indicated earlier, for all formulations except 7996, where the theoretically predicted burning rates are 10 to 20 percent high. In addition, the crossflow effect predictions agree reasonably well with the data in general. With the baseline formulation (4525), the theory slightly underpredicts the effect of crossflow on burning rate while with 5051, 4685; and 5542 (the other three non-catalyzed unimodal ozidizer formulations) agreement between theory and data is excellent. The model predicts that the high burning rate formulation (5555) should be quite insensitive to crossflow velocity, in excellent agreement with experiment. Formulation 5565, on the other hand, appears to be slightly less sensitive to crossflow than predicted, particularly at the lower pressures (1-3 MPa). Agreement between theory and data for the remaining three multimodal oxidizer, non-metalized formulations is good, except that the zero-crossflow offset between theory and data for 7996 appears to be maintained for the crossflow cases. Finally, the rather limited data for the metalized formulation (6626) appear to be in general agreement with predictions.

Results for the various formulations may be compared to identify parameters dominating the sensitivity of burning rate to crossflow. Formulations 4525, 5051, and 4685 were identical except for oxidizer particle size (and, as a consequence) base (no-crossflow) burning rate. Examination of Figures 7-9 reveals that the crossflow sensitivity increases with increasing particle size (decreasing base burning rate). For example, at 200 m/sec and 5 MPa, the augmentation ratios for 4685, 4525 and 5051 are about 1.10, 1.60 and 2.00 respectively.

Comparison of data for 4525 and 4869, differing only in use of catalyst in the latter (with consequent higher base burn rate) again shows an increase in crossflow sensitivity with decreasing base rate. At 5 MPa and 200 m/sec, their respective burn rate augmentation ratios are 1.60 and 1.10, while at 600 m/sec, the $r/r_0$ values are 2.3 and 1.7. Thus, base burn rate is seen to affect erosion sensitivity even at constant oxidizer size.

Formulations 4685 and 4869 have approximately the same base burning rate at 8 MPa although their oxidizer sizes are different. Data comparison indicates that these formulations have nearly the same sensitivity to low crossflow velocities at 8 MPa, with the catalyzed propellant being only slightly more sensitive at higher velocities. Thus, it appears that it the base burning rate rather than the oxidizer particle size which dominates the sensitivity of this series of four 73/27 AP/HTPB formulations to crossflow, though oxidizer size itself does appear to have a slight additional effect, crossflow sensitivity decreasing with decreasing size at constant base rate.

Formulation 5542 differs from 4525 in oxidizer/fuel ratio and consequently flame temperature. Since oxidizer particle size was held constant, the higher O/F ratio results in higher base rate for 5542. The data (Figure 7 and 11) indicate that the crossflow sensitivity of 5542 is considerably lower over the entire range of conditions studied. Comparison of results for 5565 and 4525, which differ in O/F ratio, but have the same base burning behavior (due to compensating AP particle size differences) indicates that the sensitivity of these two formulations to crossflow is nearly identical. Accordingly, it may be concluded that O/F ratio (and consequently flame temperature) changes do not directly effect the erosion sensitivity of these forumulations, but only affect it through their effect on base burning rate.

As indicated in Table III, Formulation 6626 (metalized) has nearly the same base burning characteristics as 4525 and 5565 and approximately the same flame temperature as 5565. The data of Figures 7, 12 and 17 reveal that all three formulations have quite similar erosive burning characteristics. For example, at 760 m/sec and 2.8 MPa, the augmentation ratios for 4525, 5565, and 6626 are 2.1, 2.25, and 2.1, while at 260 m/sec and 4.0 MPa, they are 1.65, 1.55 and 1.60. These results support a conclusion that the dominant factor affecting crossflow sensitivity of composite propellants is base burning rate, largely independent of the factors determining that base rate.

Formulations 5555, 5565, 7993, 7996, and 8019 are identical in composition (82/18 AP/HTPB) differing only in oxidizer particle size blends, which were adjusted to give a range of base (zero-crossflow) burning rate versus pressure characteristics. In Figure 18, data extracted from Figures 12-16 are plotted in the form of burning rate augmentation factor ($r/r_o$) versus base burning rate for three combinations of pressure and crossflow velocity. As may be seen, the augmentation factor decreases monotonically and fairly smoothly with increasing base burning rate, again indicating the importance of that parameter on crossflow sensitivity.

A summary of the above comparisons, delineating the effects of various parameters on crossflow sensitivity of burning rate is presented in Table IV.

## MOTOR SCALING EFFECTS

It has been observed in the past that erosive burning effects tend to diminish with increasing motor size, all other parameters being held constant. It is therefore of interest to ascertain whether the model described above can predict such a trend. Accordingly, a series of calculations have been run for equal crossflow velocities and pressures with different motor diameters. Typical results are plotted in Figures 19 and 20, comparison being made between motors with port diameters of 1.0 and 10 inches. As may be seen, erosive

burning effects are indeed predicted to decrease significantly with increasing motor size. Another point of interest may be made from Figure 20. One of the weakest links in the use of the flow profile analysis routine outlined earlier for calculation of the flame bending angle and turbulent transport property distribution is specification of the ratio of skin friction coefficient with blowing to that without blowing as a function of the blowing ratio, as discussed in detail in Reference 2. Accordingly, several different empirical expressions have been examined (See Figure 21). As shown in Figure 20, the predicted burning rate augmentation ratio is in general fairly insensitive to the choice of expression among those considered as reasonable possibilities.

## CONCLUSIONS

A fundamental composite propellant combustion model capable of predicting burning rate as a function of pressure and crossflow velocity, given only propellant composition and ingredient particle size has been developed. Testing against zero-crossflow data for a series of 13 non-catalyzed AP/HTPB formulations (4 containing aluminum additive) indicates that the model does an excellent job in predicting the non-erosive burning rate versus pressure characteristics of such formulations. In addition, erosive burning data have been obtained for 10 of these formulations: the model also does a good job in predicting the observed erosive burning behavior of these propellants.

The data obtained to date indicate that the base (no-crossflow) burning rate characteristics of the propellant have a predominant affect on its sensitivity to crossflow, high burning rate formulations being considerably less susceptible to erosive burning than low burning rate formulations, whether the base burning rate alterations are produced by oxidizer particle size variation, oxidizer/fuel ratio variation, addition of metal, or use of catalysts. Thus propellants with widely differing oxidizer size distribution, O/F ratios, metal loadings, etc tend to show identical erosive burning behavior as long as they have identical base (no crossflow) burning rate characteristics. Oxidizer particle size does appear to have some residual effect (but only a slight one) beyond its effect on base burning rate, erosion sensitivity increasing with increasing particle size. An important preliminary conclusion is that aluminum (at least at low levels) does not affect erosion sensitivity other than through its effect on base burning rate.

The model also predicts a decrease in erosive effects with increasing motor port size (at equal pressure and crossflow velocity) in agreement with observations by other investigators.

## REFERENCES

1. King, M., "Model for Steady State Combustion of Unimodal Composite Solid Propellants," AIAA Paper 78-216, Jan., 1978. Available from Engineering Socieities Library, 245 East 47th Street, NY, NY 10017.

2. King, M., "A Model of the Effects of Pressure and Crossflow Velocity on Composite Propellant Burning Rate," AIAA Paper 79-1171, June, 1979. Available from Engineering Societies Library, 345 East 47th Street NY, NY 10017.

3. Beckstead, M.W., Derr, R.L. and Price, C.F. Thirteenth Symposium (International) on Combustion, p. 1047, the Combustion Institute, 1971.

4. Waesche, R.H.W. and Wenograd, J., "Calculation of Solid Propellant Burning Rates from Condensed-Phase Decomposition Kinetics," AIAA Paper 69-145, January 1969. Available from Engineering Societies Library, 345 East 47th Street, NY, NY 10017.

5. Burke, S.P. and Schumann, T.E.W., Ind Eng Chem, 20, 998 (1928); also First/Second Symposium Combustion, p. 2, The Combustion Institute, Reprinted 1965.

6. Glick, R.L. and Condon, J.A., "Statistical Analysis of Polydisperse, Heterogeneous Propellant Combustion: Steady-State," 13th JANNAF Combustion Meeting, CPIA Publication No. 281, Vol. II, p. 313, December, 1976.

7. Beckstead, M.W., "A Model for Solid Propellant Combustion," 14th JANNAF Combustion Meeting, CPIA Publication No. 292, Vol. I, p. 281, December, 1977.

8. Belyaev, A.F., Frolov, Yu.V., and Korotkov, A.I., Fizika Goreniya i Vzryva, 4, 3, 323-329 (1968).

9. Marshall, R.L., Pellet, G.L. and Saunders, A.S., "An Experimental Study of the Drag Coefficient of Burning Aluminum Droplets," Air Force Rocket Propulsion Laboratory Report AFRPL-TR-67-223, Vol II, p. 843, August, 1967.

10. King, M.K. "Erosive Burning of Composite Solid Propellants," 15th JANNAF Combustion Meeting, CPIA Publication 297, Vol. II, p. 179-188, February, 1979.

11. King, M.K., "An Investigation of the Effects of Formulation Parameters On Erosive Burning of Composite Propellants," 16th JANNAF Combustion Meeting, Monterey, California, September, 1979. CPIA Publication 308, Vol. II, pp. 171-191, December 1979.

12. King, M., "Erosive Burning of Composite Propellants," 13th JANNAF Propulsion Meeting, CPIA Publication 281, Vol. II, p. 407, December, 1976.

Table I. Main Equations used in Flow Profile Analysis (Coupled with Burning Rate Analysis Through Temperature Dependence of Density and Viscosity).

1. $C_{f0} = f_1 (Re, D_e/k)$

2. $C_f/C_{f0} = f_2 (B) \qquad B = (\dot{m}_{inj}/\dot{m}_{crossflow})/(C_{f0}/2)$

3. $\tau_{wall} = (C_f/2)\ \rho_{fs}\ U_{fs}^2$

4. $\tau_y = \tau_{wall} + \dot{m}_{inj}\ U - K_{mom\ int}\ Y$

5. $\tau_{\dot{y}} = (\mu + \rho\epsilon)\ dU/dY$

6. $\epsilon = \left[f_3\ (Y, m_{inj}, dP/dx, k)\right]\ dU/dY$

   FOR ZERO ROUGHNESS AND NO DAMPING, FOR EXAMPLE

   $\epsilon = .168\ Y^2\ (dU/dY)$

7. $\rho = P(MW)/RT$

8. $\mu = kT^{0.8}$

9. $T = T_s + (T_f - T_s)Y/(L_{R\dot{X}} + FH90 \sin\theta)$

10. $V = \dot{m}_{inj}/\rho$

Table II. Application of Flow Profile Analysis Equations.

1. USE EQNS 1-4 TO OBTAIN $\tau = g(u,y)$
2. *INTEGRATE EQN 5, WITH USE OF EQNS 4 AND 6-9, FROM THE WALL (SURFACE) TO OBTAIN u, du/dy, $\epsilon$ AS FUNCTION OF y
3. KNOWING c(y), COMBINE THIS WITH EQNS 7-9 TO OBTAIN $[1 + \rho c/\mu]$ AS A FUNCTION OF y
4. USE THIS FUNCTION TO OBTAIN AVERAGE AUGMENTATION RATIOS FOR LAMINAR TRANSPORT PROPERTIES OVER VARIOUS REGIONS AND USE THESE TO ADJUST EFFECTIVE FLAME OFFSET DISTANCES
5. HAVING u(y) AND v(y) INTEGRATE ALONG A STREAMLINE TO DETERMINE THE EFFECTIVE REDUCTION OF DIFFUSIONAL DISTANCE DUE TO FLAME BENDING.
6. LOOP – FAIRLY COMPLEX FOR UNIMODAL AP CASES; EVEN MORE SO FOR MULTIMODAL AP CASES, WHERE INTERACTION BETWEEN THE MODES MUST NOW BE CONSIDERED

*FOR LOW CROSS FLOW, HIGH BLOWING RATIO CASES, THE -Ky TERM IN EQN4 CAUSES $\tau$ TO GO NEGATIVE, A RESULT WE INTERPRET AS INDICATING BOUNDARY LAYER BLOWOFF – IF THIS OCCURS, WE USE A COSINE LAW VELOCITY PROFILE FOR OUR ANALYSIS IN PLACE OF INTEGRATION OF EQN 5.

## Table III. Propellant Matrix (AP/HTPB) Tested.

| FORMULATION | COMPOSITION | RATIONALE |
|---|---|---|
| 4525 | 73/27 AP/HTPB, 20 MICRON AP | BASELINE FOMULATION, FLAME TEMPERATURE = 1667°K |
| 5051 | 73/27 AP/HTPB, 200 MICRON AP | COMPARE WITH 4525 FOR AP SIZE EFFECT AND BASE BURNING RATE EFFECT |
| 4685 | 73/27 AP/HTPB, 5 MICRON AP | COMPARE WITH 4525 AND 5051 FOR AP SIZE EFFECT AND BASE BURNING RATE EFFECT |
| 4869 | 72/26/2 AP/HTPB/$Fe_2O_3$, 20 MICRON AP | COMPARE WITH 4525 FOR BASE BURNING RATE EFFECT AT CONSTANT AP SIZE |
| 5542 | 77/23 AP/HTPB, 20 MICRON AP | COMPARE WITH 4525 FOR MIXTURE RATIO AND FLAME TEMPERATURE EFFECT AT CONSTANT AP SIZE. T=2065°K |
| 5565 | 82/18 AP/HTPB, 13.65% 90 MICRON AP, 68.35% 200 MICRON AP | AP SIZES CHOSEN TO MATCH BASE BURNING RATE OF 4525. COMPARE WITH 4525 FOR MIXTURE RATIO AND FLAME TEMPERATURE EFFECT. T=2575°K |
| 5555 | 82/18 AP/HTPB, 41% 1 MICRON AP, 41% 7 MICRON AP | COMPARE WITH 5565 FOR EFFECT OF BASE BURNING RATE. |
| 7993 | 82/18 AP/HTPB, 41% 7 MICRON AP, 41% 90 MICRON AP | FURTHER STUDY OF AP SIZE AND BASE BURNING RATE EFFECTS |
| 7996 | 82/18 AP/HTPB, 41% 20 MICRON AP, 41% 200 MICRON AP | |
| 8019 | 82/18 AP/HTPB, 27.3% 1 MICRON AP, 27.3% 20 MICRON AP, 27.4% 200 MICRON AP | |
| 6626 | 74/21/5 AP/HTPB/Al, 70% 90 MICRON AP, 4% 200 MICRON AP | SAME FLAME TEMPERATURE AND BASE BURNING RATE AS 5565. COMPARE WITH 5565 FOR Al EFFECT. |
| 8495 | 73/17/10 AP/HTPB/Al, 7.3% 90 MICRON AP, 58.4%, 200 MICRON AP, 7.3%, 400 MICRON AP | STUDY OF EFFECTS OF VARIOUS ALUMINUM LOADINGS AND O/F RATIOS ON EROSIVE BURNING BEHAVIOR. |
| 8497 | 80/15/5 AP/HTPB/Al, 8.0% 90 MICRON AP, 64.0%, 200 MICRON AP, 8.0% 400 MICRON AP | |
| WC19M | 70/12/18 AP/HTPB/Al, 21.0% 20 MICRON AP, 39.0%, 90 MICRON AP, 10.0%, 200 MICRON AP | |

## Table IV. Effects of Various Parameters on Sensitivity of Formulations to Crossflow.

| COMPARISON | PARAMETERS STUDIED | EFFECT ON EROSIVE BURNING |
|---|---|---|
| 4525, 5051, 4685 | VARIED $d_p$, $r_0$ AT FIXED BINDER TYPE, FIXED FLAME TEMPERATURE | $d_p \downarrow \leftrightarrow r_0 \downarrow \rightarrow \varepsilon \downarrow$ |
| 4524, 4869 | VARIED $r_0$ AT FIXED AP SIZE, BINDER TYPE, AND FLAME TEMPERATURE | $r_0 \downarrow \rightarrow \varepsilon \downarrow$ |
| 4685, 4869 | VARIED $d_p$ AT FIXED $r_0$, BINDER TYPE, AND FLAME TEMPERATURE | $d_p \downarrow \rightarrow \varepsilon \downarrow$ SLIGHTLY |
| 4525, 5542 | VARIED O/F RATIO (AND THUS FLAME TEMPERATURE) AND $r_0$ AT FIXED BINDER TYPE AND FIXED AP SIZE | $T_f \downarrow \leftrightarrow r_0 \downarrow \rightarrow \varepsilon \downarrow$ |
| 5565, 4525 | VARIED O/F RATIO (AND THUS FLAME TEMPERATURE) AT FIXED BINDER TYPE AND FIXED $r_0$ | $T_f \downarrow \rightarrow \varepsilon$ UNCHANGED |
| 5565, 5555, 7993 7996, 8019 | VARIED $d_p$, $r_0$ AT FIXED BINDER TYPE, FIXED FLAME TEMPERATURE | $d_p \downarrow \leftrightarrow r_0 \downarrow \rightarrow \varepsilon \downarrow$ |
| 5565, 6626 | ALUMINUM VERSUS NON ALUMINUM AT FIXED $r_0$ BINDER TYPE, AND FLAME TEMPERATURE | $\varepsilon$ UNCHANGED |

CONCLUSIONS FROM ABOVE COMPARISONS

1. THE AUGMENTATION FACTOR IS STRONGLY DEPENDENT ON BASE BURNING RATE.
2. THERE IS A SMALL RESIDUAL EFFECT OF OXIDIZER PARTICLE SIZE, AT FIXED BURNING RATE.
3. O/F (FLAME TEMPERATURE) EFFECTS $\varepsilon$ FOR HTPB SYSTEMS ONLY THROUGH EFFECT ON BASE BURNING RATE.
4. AT FIXED BASE BURNING RATE, ALUMINUM HAS NO EFFECT ON $\varepsilon$.

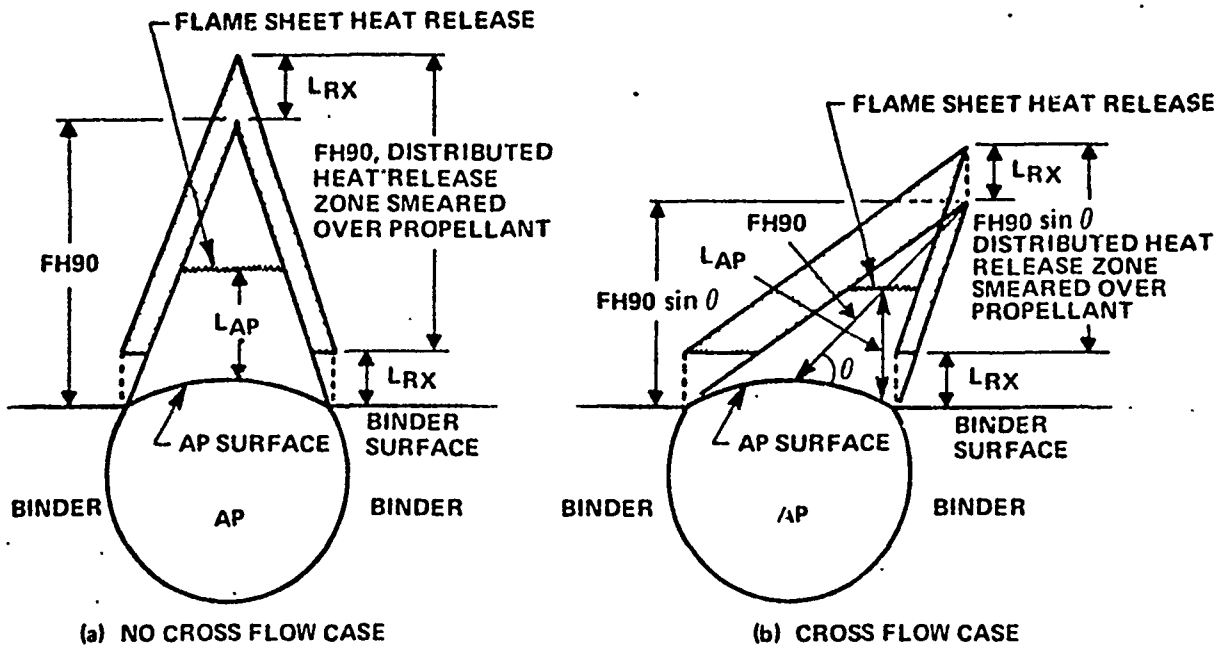


Figure 1. Schematic of Burning Composite Propellant Postulated Flame Structure, with and without Crossflow.

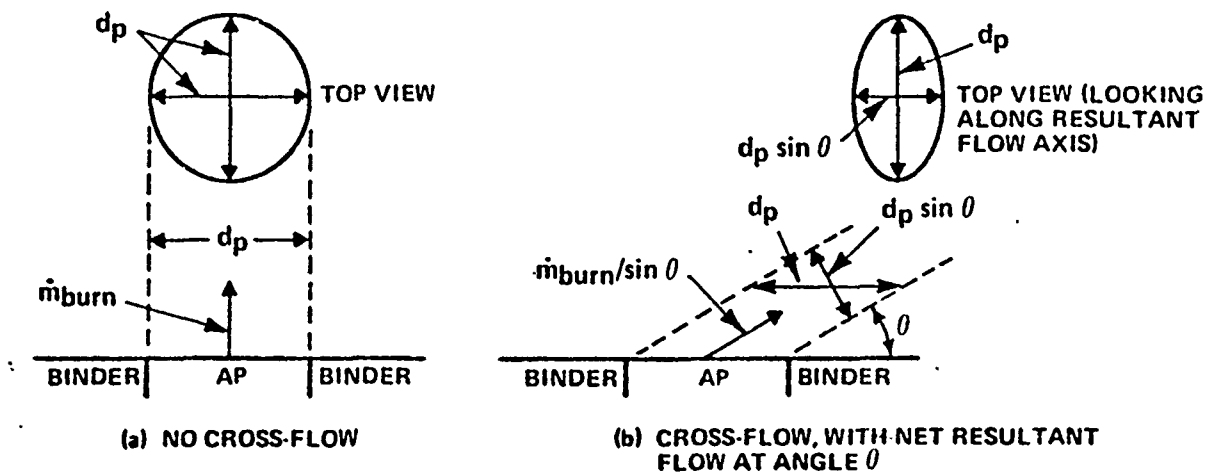


Figure 2. Modification of Diffusion Flame Shape by Crossflow.

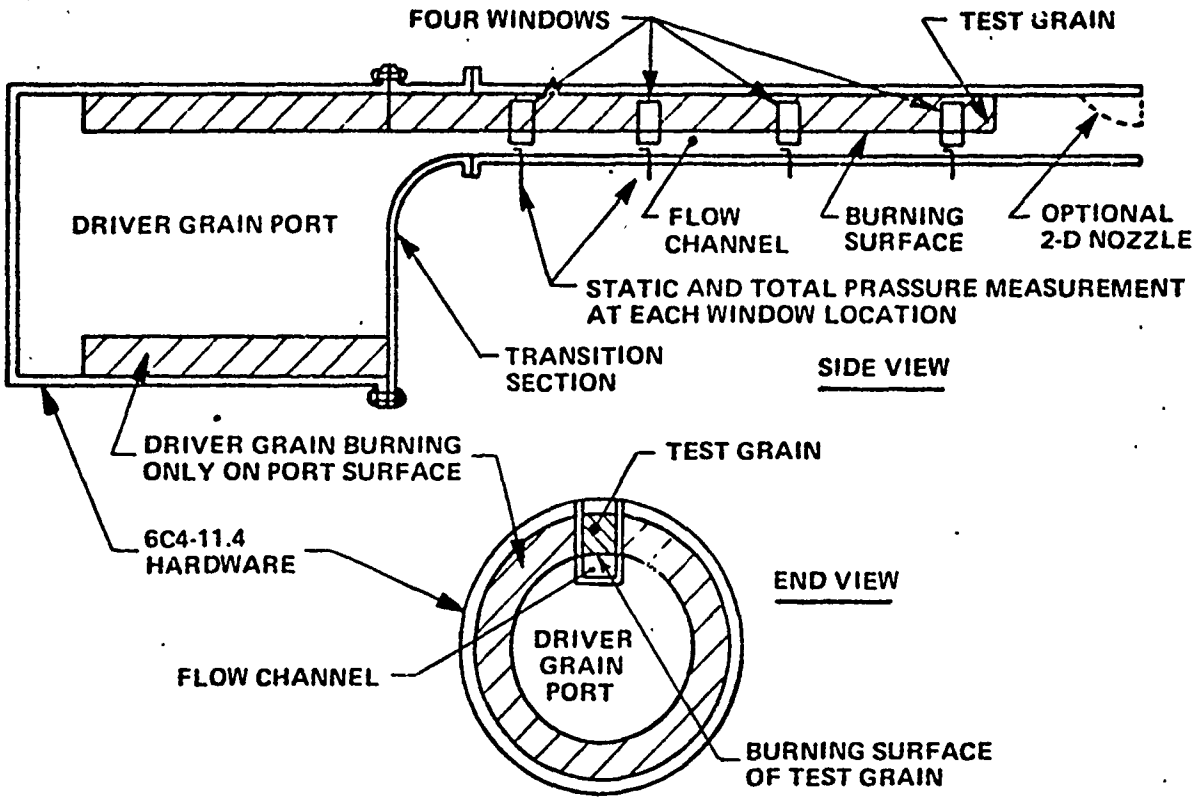


Figure 3. Schematic Drawing of Erosive Burning Test Apparatus.

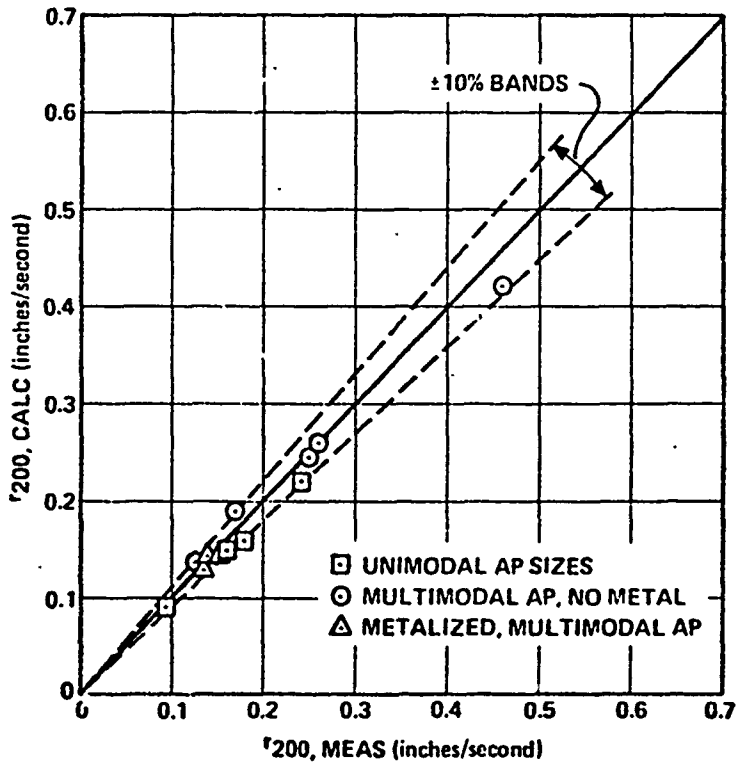


Figure 4. Zero-Crossflow Burning Rates at 200 psia, Data and Predictions.

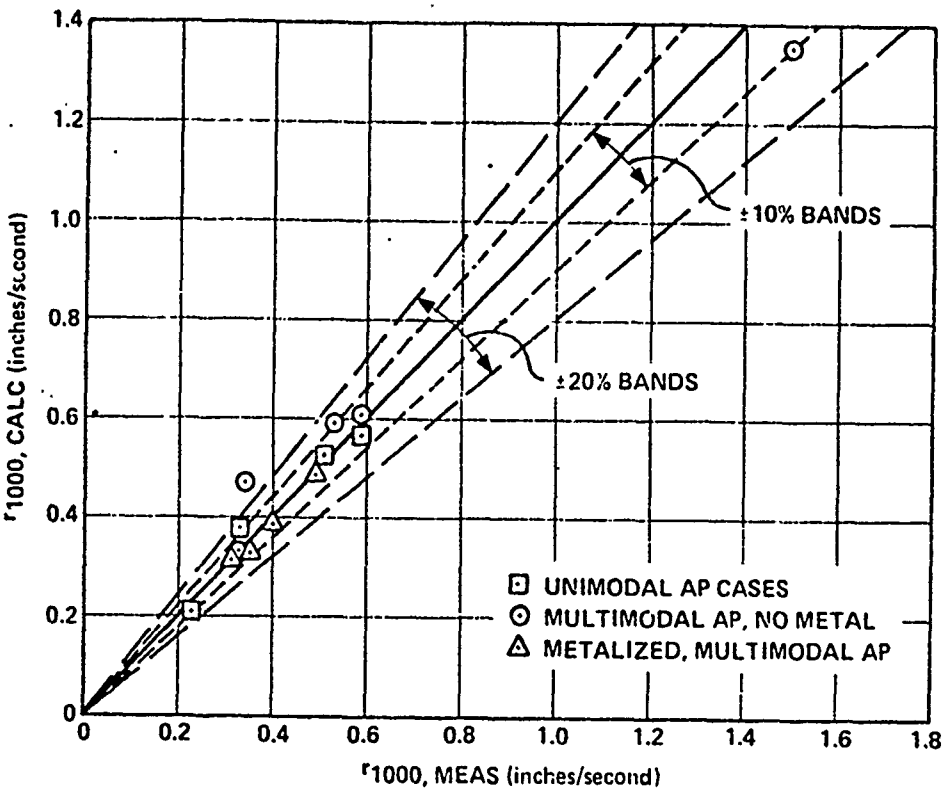


Figure 5. Zero-Crossflow Burning Rates at 1000 psia, Data and Predictions.

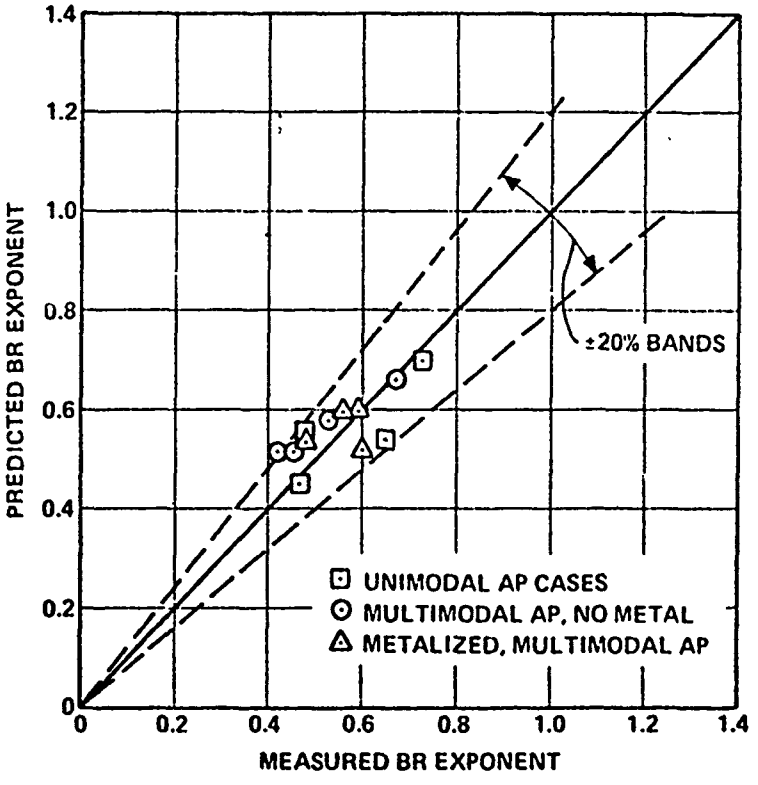


Figure 6. Zero-Crossflow Burning Rate—Pressure Exponent at 1000 psia, Data and Predictions.

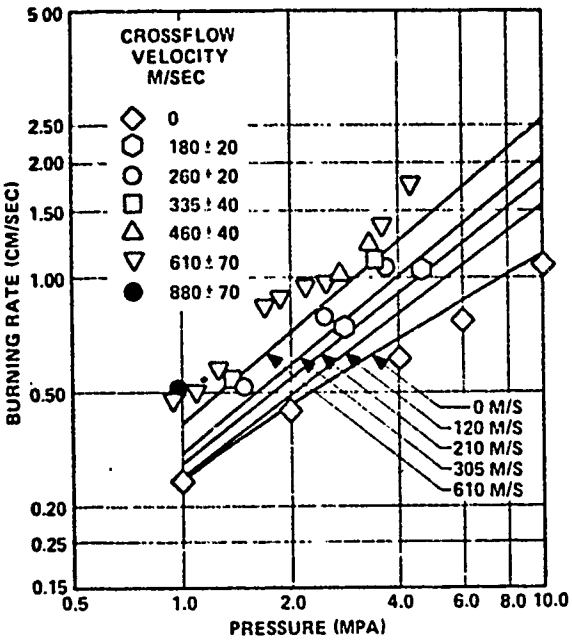


Figure 7. Burning Rate Predictions (Solid Lines) and Data (Points) for Formulation 4525 (73/27 AP/HTPB, 20 MICRON AP).

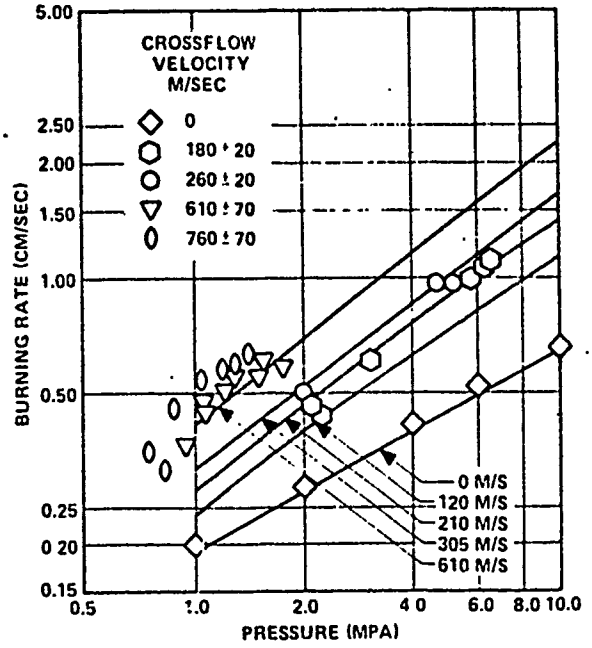


Figure 8. Burning Rate Predictions (Solid Lines) and Data (Points) for Formulation 5051 (73/27 AP/HTPB, 200 Micron AP).

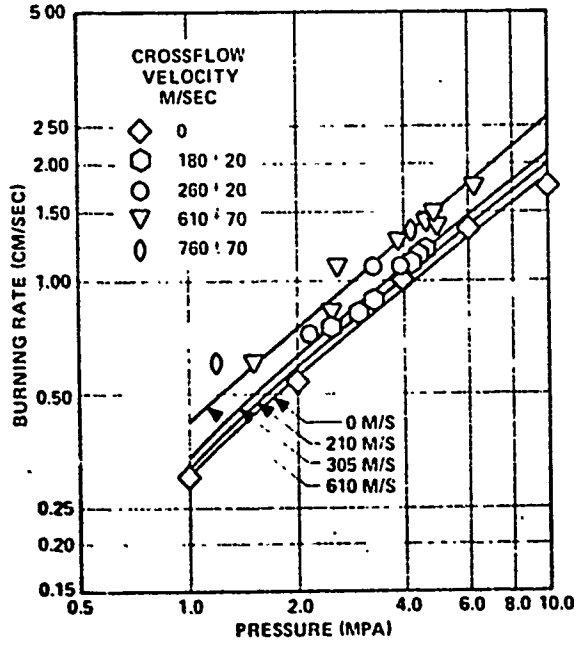


Figure 9. Burning Rate Predictions (Solid Lines) and Data (Points) for Formulation 4685 (73/27 AP/HTPB, 5 Micron AP).

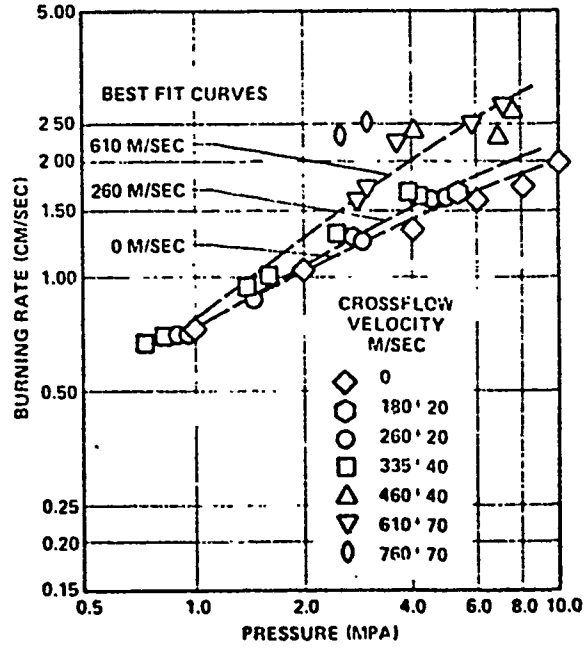


Figure 10. Burning Rate (No Predictions) for Formulation 4869 (72/26/2 AP/HTPB/$Fe_2O_3$, 20 Micron AP).

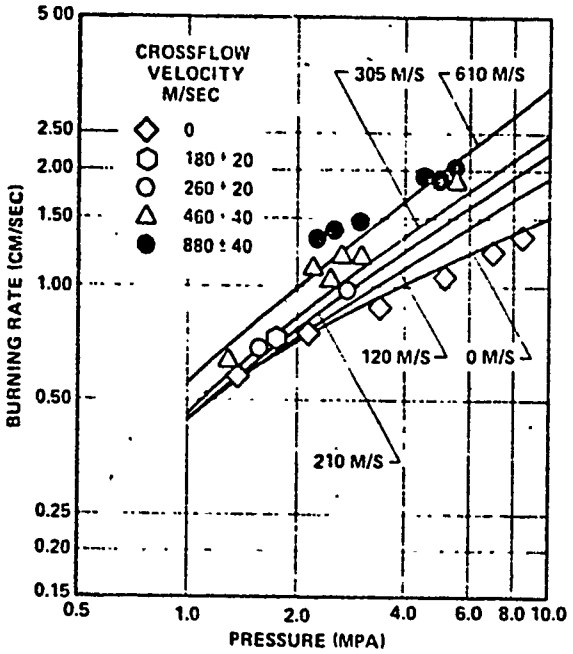


Figure 11. Burning Rate Predictions (Solid Lines) and Data (Points) for Formulation 5542 (77/23 AP/HTPB, 20 Micron AP).

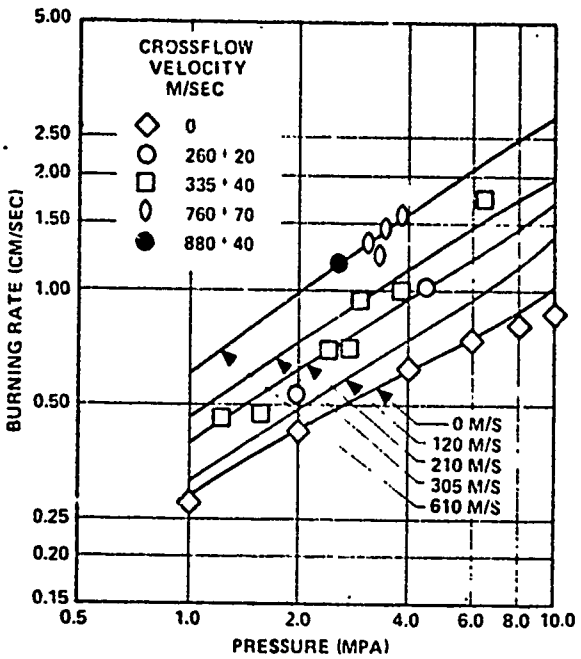


Figure 12. Burning Rate Predictions (Solid Lines) and Data (Points) for Formulation 5565 (82/18 AP/HTPB, 13.65% 90 Micron AP, 68.35% 200 Micron AP).

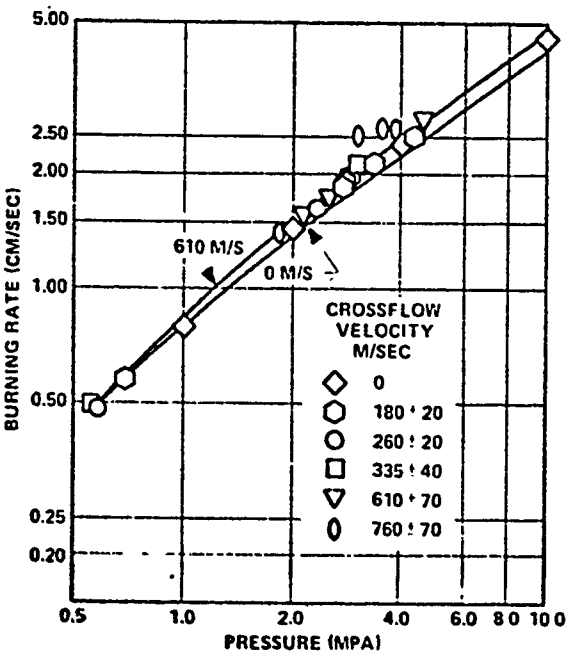


Figure 13. Burning Rate Predictions (Solid Lines) for Formulation 5555 (82/18 AP/HTPB, 41% 1 Micron AP, 41% 7 Micron AP).

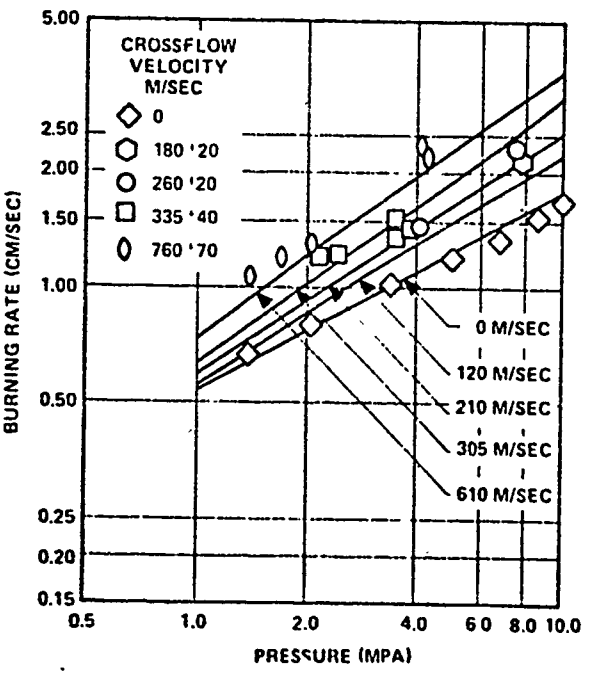


Figure 14. Burning Rate Predictions (Solid Lines) and Data (Points) for Formulation 7993 (82/18 AP/HTPB, 41% 7μ AP, 41% 90μ AP).

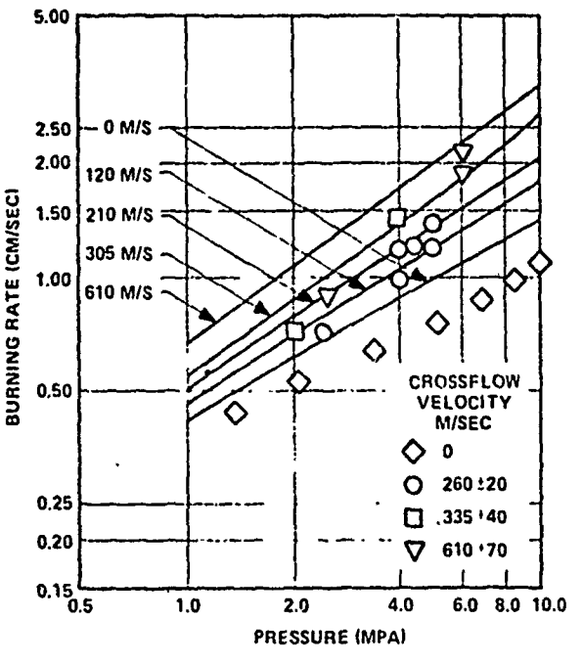


Figure 15. Burning Rate Predictions (Solid Lines) and Data (Points) for Formulation 7996 (82/18 AP/HTPB, 41% 20μ AP, 41% 200μ AP).

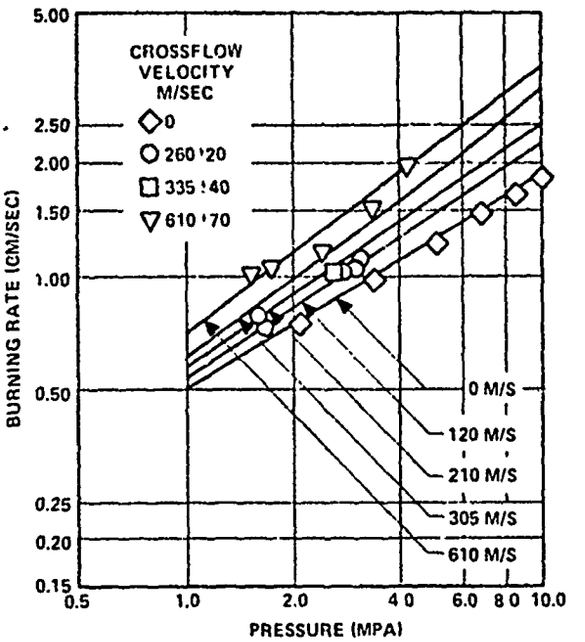


Figure 16. Burning Rate Predictions (Solid Lines) for Formulation 8019 (82/18 AP/HTPB, 27.3% 1μ AP, 27.3% 20μ AP, 27.4% 200μ AP).

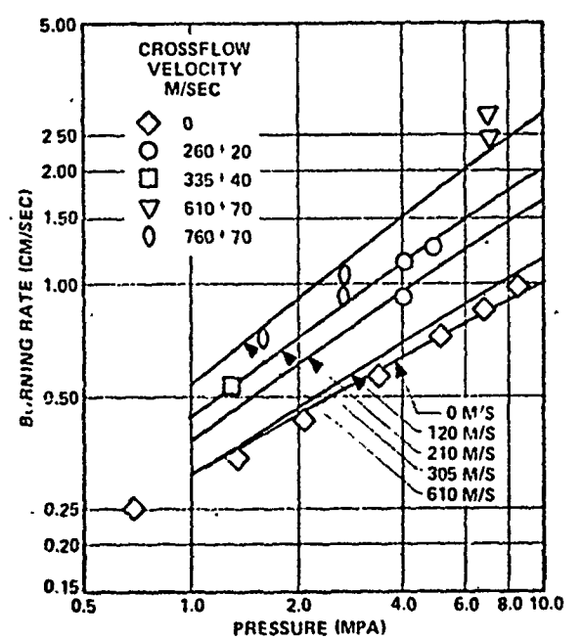


Figure 17. Burning Rate Predictions (Solid Lines) and Data (Points) for Formulation 6626 (74/21/5 AP/HTPB/Al, 5 Micron Al, 70% 90 Micron AP, 4% 200 Micron AP).

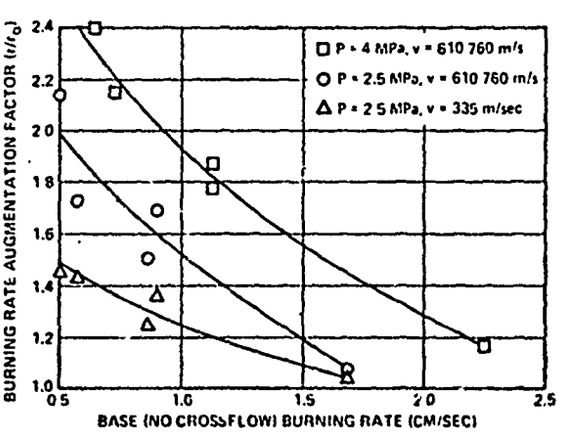


Figure 18. Summary of Results for 82/18 AP/HTPB Formulations.

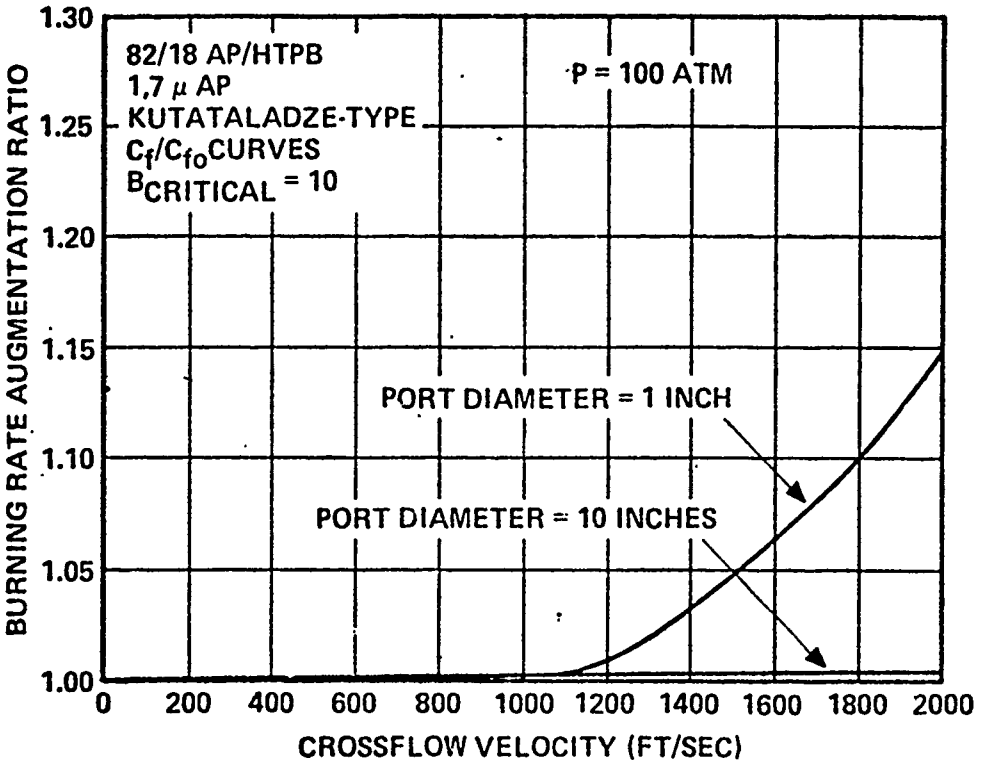


Figure 19. Scaling Effects on Predicted Erosive Burning.

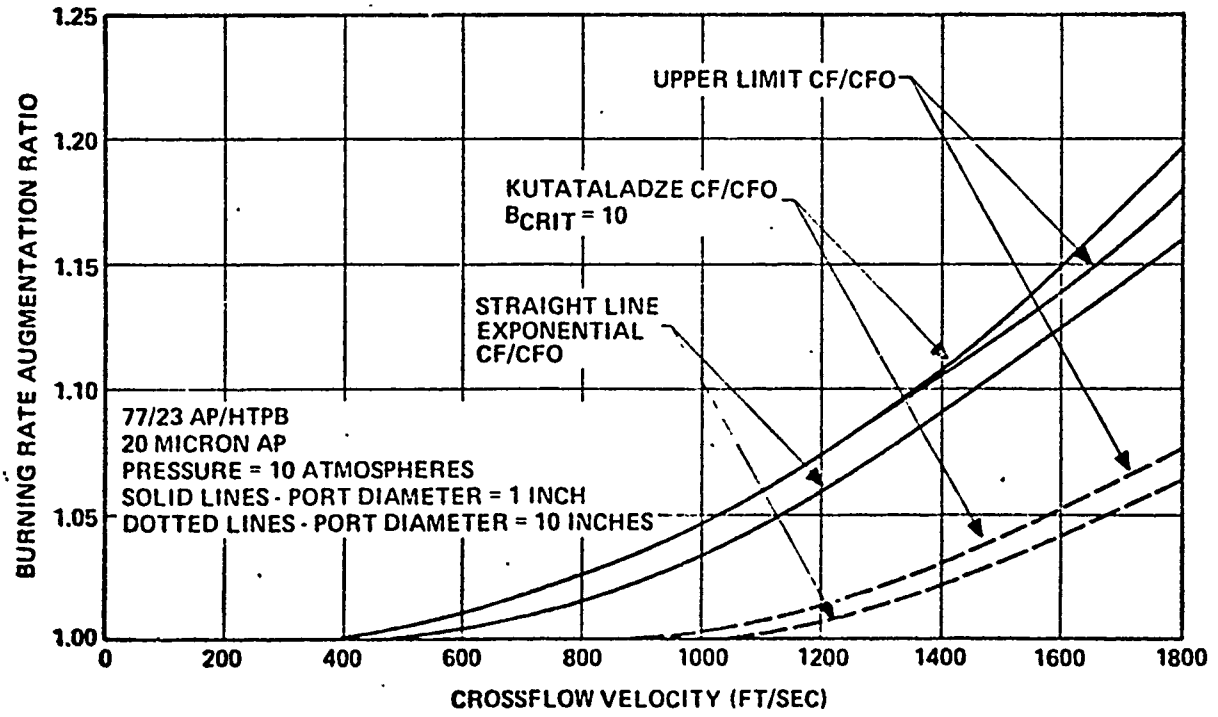


Figure 20. Scaling Effects on Predicted Erosive Burning.

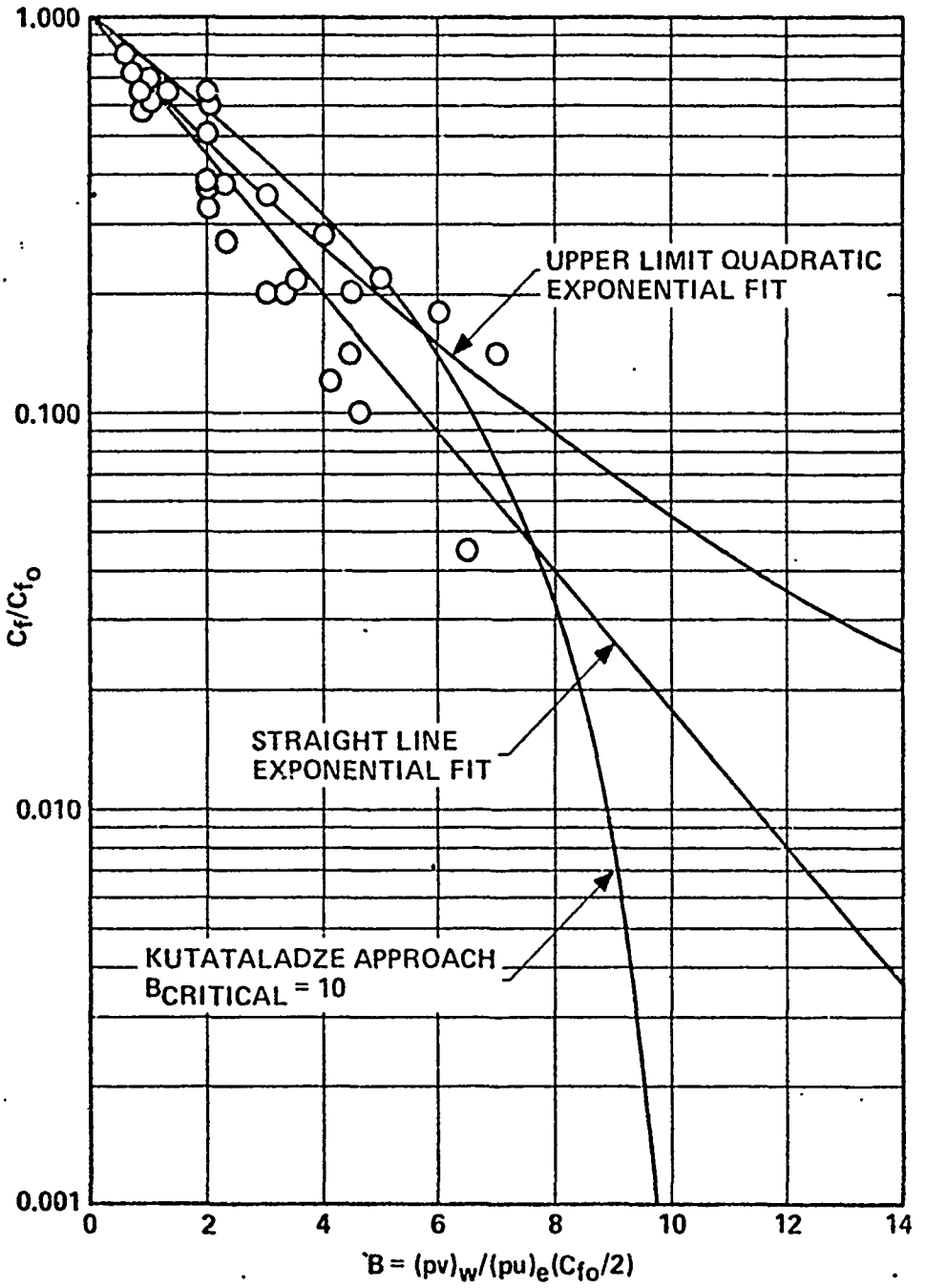


Figure 21. Skin Friction Coefficient Reduction Versus Blowing Parameter.